Indian Journal of Chemical Technology
Vol. 24, July, 2017 pp. 383-392

Kinetic and thermodynamic studies of Direct Red 23 removal using zero-valent nanoparticles immobilized on multi walled carbon nanotubes from aqueous solution

Nafiseh Mansouriieh*,[1] & Mahmoud Reza Sohrabi[2]

[1]Young Researchers and Elite Club,Tabriz Branch, Islamic Azad University Tabriz, Islamic Republic of Iran

[2]Department of chemistry, Islamic Azad University, North Tehran Branch, P.O Box 1913674711, Tehran, I. R. Iran

E-mail: nafisehmansoriieh@gmail.com

Received 28 June 2015; accepted 6 April 2017

In the present study nanoscale zero valent iron (nZVI) has been immobilized on multi-walled carbon nanotubes (MWCNTs) and used to remove Direct Red 23 (DR 23) from aqueous solution. The effect of parameters such as, initial dye concentration, solution *p*H, adsorbent content, temperature and contact time on the adsorption process have been investigated. The studied adsorbent exhibits high efficiency for dye adsorption and the equilibrium state is achieved in 6 min. For equilibrium studies, three isotherm models, namely Langmuir, Freundlich and Temkin are used. It is found that Langmuir fits very well with experimental data. The kinetic studies suggest the process following pseudo second-order kinetics and involvement of the particle-diffusion mechanism. The value of different thermodynamic parameters, like Gibb's free energy change, enthalpy change and entropy change of the adsorption process have also been evaluated. The adsorption of DR 23 has been found to be endothermic.

Keywords: Adsorption kinetics, Direct Red 23, Isotherm model, Multi-walled carbon nanotubes, Thermodynamic parameter, Zero-valent iron nanoparticles

Effluents released from textile, paper, and printing industries contain a variety of dyes. These dyes affect the quality of the water supply because they are widely used and are toxic in nature[1]. The most group of commercial dyes used in textile industries are azo dyes. Azo dyes are characterized by (−N=N−) bound to sp^2 hybrid carbon atoms that mainly bind to benzene and naphthalene rings[2].

Azo pigments are water soluble and polar because of the presence of a sulfonic acid group in their structures[3]. Their complex aromatic structure and stability make them difficult to remove using traditional wastewater treatment processes; the dyes are known as mutagenic and carcinogenic compounds[4].

Low cost zero-valent iron (ZVI) is a powerful reducing agent. It is easily accessible, effective for remediation of pollutants, generates very little waste and secondary pollutants[5]. The application of nanoscale zero-valent iron (nZVI) for treatment of hazardous and toxic waste has increased because of their smaller particle size, large specific surface area and higher density of reactive surface sites[6]. Recently, these nano-particles have become increasingly important for environmental treatments, especially of contaminants such as heavy metals[7] and dyes[8]. ZVI nanoparticles convert azo dye into products that are more susceptible to biological degradation[9].

Studies have shown that the addition of porous materials, such as chitosan beads[10] and carboxymethyl cellulose[11], usually improves the stability of nZVI in aqueous systems. Carbon nanotubes (CNTs) have a unique chemical structure and are one-dimensional macromolecules that possess outstanding thermal and chemical stability[12].

In recent years, CNTs have also been used as superior adsorbents to remove contaminates. Their large specific surface area, small size, and hollow and layered structures make CNTs useful adsorbents for the removal of lead[13] and dyes[14] from aqueous solutions. CNTs demonstrate excellent support because they have a large specific area; this is helpful for the adsorption of pollution because

heterogeneous catalytic degradation of chemicals in aqueous media requires adsorption on the catalyst before degradation[15].

The present study used multi-walled carbon nanotubes (MWCNTs) as a porous-based support material for nZVI nanoparticles. The nZVI/MWCNT nanocomposite was used for the removal of anionic dye, Direct Red 23 (DR 23) from aqueous solution. In order to design on the adsorption treatment system, knowledge of the kinetic is essential. Thermodynamic parameters, ΔG^o, ΔH and ΔS, were also calculated.

Experimental Section

Chemicals

Diazo dye DR 23 (Fig. 1) (Molecular formula $C_{35}H_{27}N_7S_2O_{10}Na_2$; color index 29, 160, molar mass 813.72, UV-visible (λ_{max}): nm 500 nm) was purchased from Alvan Sabet (Iran). Ferric chloride hexa-hydrate ($FeCl_3.6H_2O$) and sodium borohydride ($NaBH_4$) were obtained from Merck (Germany). Sodium hydroxide (NaOH) and hydrochloric acid (HCl) were used for pH adjustment (Merck, Germany). MWCNTs (outer diameter 8-15 nm; inner diameter 3-5 NM; length ~50 μm; purity >95%; surface area 233 m^2/g) were obtained from Neutrino Nanovation (Iran).

Preparation of nZVI/ MWCNTs

The nZVI/MWCNTs nanocomposite was prepared by mixing ferric chloride (1.5 g) and MWCNTs (0.75 g) in 250 mL water. Sodium borohydride solution (0.3 M) was then added dropwise to the mixture. The product was stirred vigorously using a mechanical stirrer. The experiments were carried out under N_2 atmosphere and all aqueous solutions were prepared using distilled deionized water (DDW). The nZVI particles appeared immediately after introducing the first drop of solution. The stabilized iron particles were separated by filtration and washed with DDW. The resulting reaction was[16]:

$$4Fe^{3+}_{(aq)} + 3BH^-_4 + 9H_2O \rightarrow 4Fe^0 + 3H_2BO^-_{3(aq)} + 12H^+_{(aq)} + 6H_{2(g)} \quad \text{... (1)}$$

A scanning electron microscope (Philips, ESEM, XL 30) was used to characterize the nZVI/MWCT nanocomposite for its morphological information.

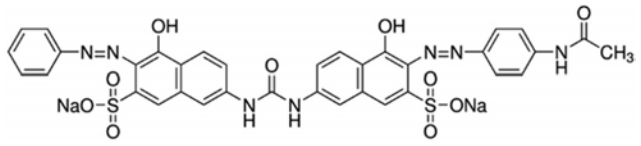

Fig. 1 — Direct Red 23 diazo dye.

Batch experiments

Adsorption of DR 23 dye by nZVI/MWCT nanocomposite was carried out by batch method and the influence of various parameters like contact time (min), adsorbent dosage (1-4 g/L), *p*H (4-8), initial DR 23 dye concentration (20-50mg/L) and temperature (293, 303 and 313 K) were studied. The adsorption measurements were conducted by mixing various amounts of nZVI/MWCT nanocomposite in glass Erlenmeyer flasks containing 50 mL of dye solution with known concentration. The *p*H of the solution was adjusted to the desired value by adding a small amount of HCl (0.1 M) or NaOH (0.1 M). Optimum nZVI/MWCNs mass ratio for DR 23 dye removal was determined at 1:3[17].

At the end of determined time intervals, the samples were taken out and the supernatant solution was separated from the nZVI/MWCT nanocomposite by centrifugation at 3000 rpm for 15 min (Kokusanh; 108 N). The reaction was followed by a double-beam UV-vis spectrometer equipped with a 1 cm quartz cell (Cary 100; Varian) and the adsorption yield (R%) and amount of DR 23 per unit of adsorbent (q_e) was calculated using Eqs. (3) and (4), respectively[18,19]:

$$R\ (\%) = \frac{C_0 - C_t}{C_0} \times 100 \quad \text{... (2)}$$

$$q_e = \frac{(C_0 - C_e)V}{W} \quad \text{... (3)}$$

where C_0 is the initial DR 23 concentration in the solution (mg/L) and C_t is the DR 23 concentration at *t* min (mg/L), C_e is equilibrium concentration of DR 23 (mg/L), V is the volume of dye (L); and W is the weight of adsorbent (g).

Results and Discussion

Characterization of nZVI/MWCNTs composites

Figure 2(a) shows the XRD diffractogram of the synthesized nZVI particles and shows that the characteristic 2θ value was 44.54°. These diffraction patterns indicate that the iron present in the sample is mainly in a zero-valent state. Figure 2(b) shows the nZVI/MWCNTs composite XRD pattern. It indicates that the nZVI-MWCNTs maintained their typical MWCNT structure and the framework remained intact. The typical peaks for MWCNT appeared at 2θ of 43° and Fe^0 of 44.55°. An apparent peak at 2θ = 44.55° indicates the presence of nZVI, which confirms that the nZVI nanoparticles either load outside the carbon nanotubes or inside the pores and cracks of the network.

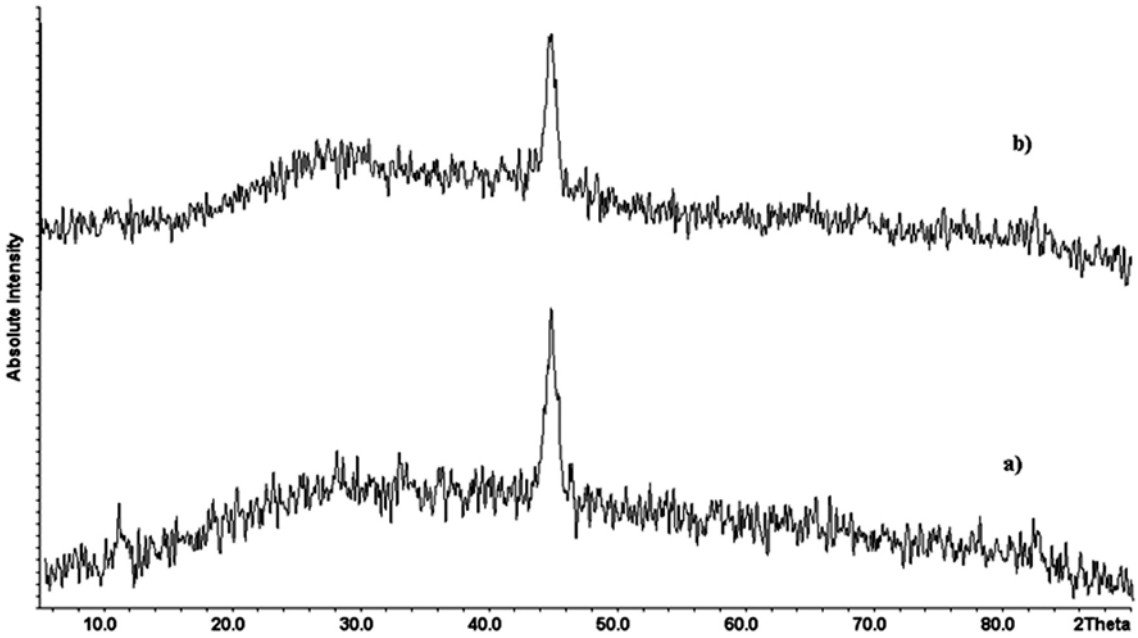

Fig. 2 — XRD patterns of (a) synthesized nZVI, (b) nZVI/MWCNTs composite.

The adsorption ability of MWCNT has been attributed to its rich surface area. The specific surface area of the MWCNTs used in this study was 233 m^2/g. Figure 3(a, b) shows the morphology and size of the ZVI/MWCNT nanocomposite. The bright spherical spots on the surface and inside the smooth lattice confirm nZVI nanoparticle loading onto the MWCNTs. It was evident that the addition of nZVI to MWCNTs blocked the surface of MWCNTs and decreased the adsorption capacity of the MWCNTs. Aggregation of nZVI particles was not observed, which indicated that aggregation of Fe^0 nanoparticles was well-controlled by the presence of the MWCNTs and that the MWCNTs played a significant role the support and stabilization of the nZVI[14]. The SEM images show that the ZVI particles had diameters of 28 to 60 nm.

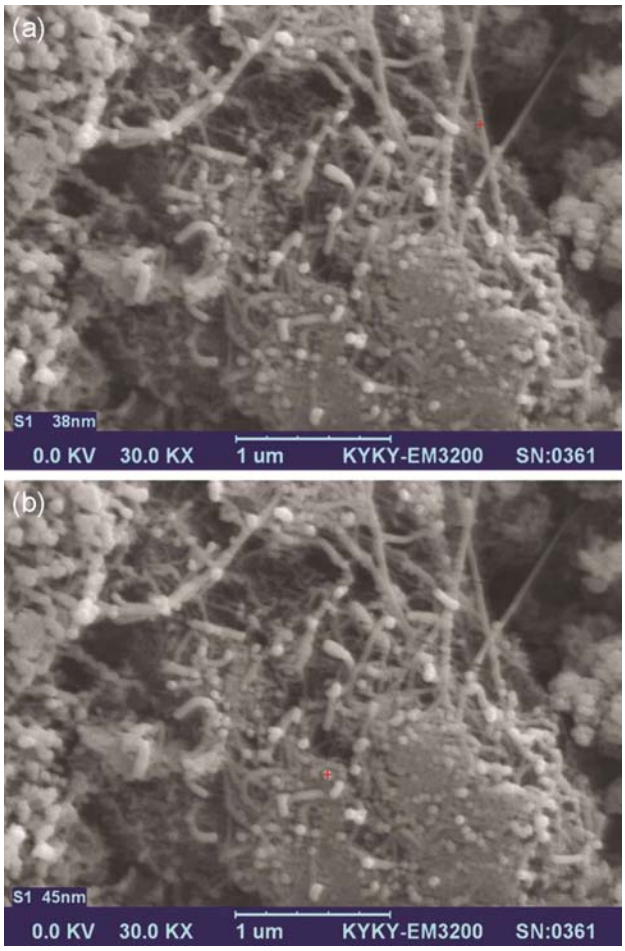

Fig. 3 — SEM images of nZVI/MWCNTs composite (a) 38 nm (b) 45 nm.

Adsorption studies

Effect of initial solution concentration on DR 23 removal

The effect of initial DR 23 concentration on color adsorption was studied using nZVI/MWCNT particles at initial concentrations of 20 to 50 mg/L.

The DR 23 uptake mechanism is particularly dependent on the initial concentration of DR 23 dye. Figure 4 shows that the adsorption of DR 23 increases with increasing initial concentration of DR 23. This is probably due to a higher mass transfer driving force as a result of the increase in the number of molecules competing for the available binding sites

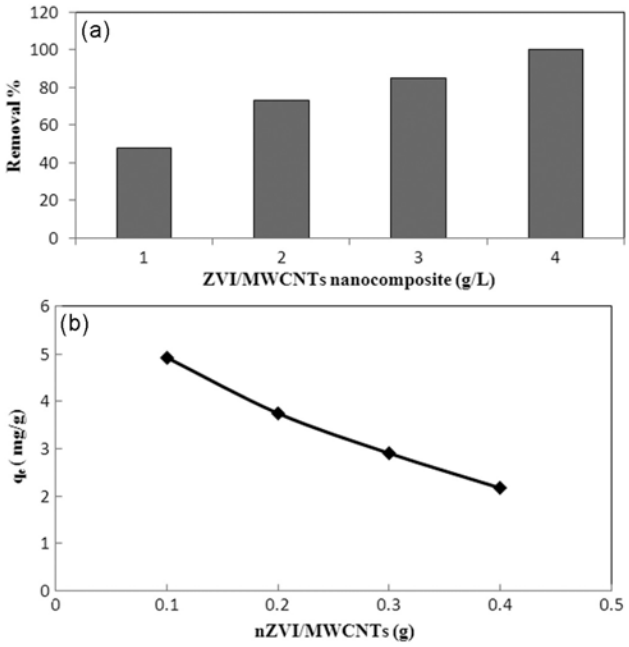

Fig. 4 — Effect of nZVI/MWCNTs content (a) on the dye removal efficiency (b) adsorption capacity ([DR 23] =20 mg/L, *p*H=4, T=293 K).

on the adsorbent when the initial concentration of DR 23 is increased[20].

Effect of nanocomposite content on DR 23 removal

Figure 4(a) shows the effect of nZVI/MWCNTs content on the dye removal efficiency. The increased nZVI/MWCNTs content in the degradation reaction increased degradation efficiency.

An increase in the nZVI/MWCNT content increased the dye removal rate. Since degradation of DR 23 occurred on the surface of the nanoparticles, the increase in nZVI/MWCNT content simultaneously increased the number of active sites and reactive surface areas, accelerating the degradation of DR 23[12]. Although as shown in Fig. 4(b), the adsorption capacity of nZVI/MWCNT nanoparticles decreases with an increase in the adsorbent dosage of nZVI/MWCNT. This reduction can be due to the aggregation of adsorbent surface and an increase in diffusion path length[21].

Effect of initial pH of solution on DR 23 removal

The adsorption of DR 23 by nZVI/MWCNTs was conducted at initial *p*H values of 4 to 8. Figure 5 shows that the adsorption capacity of dye by nZVI/MWCNTs increased as the *p*H decreased. This may a result of the electrostatic interaction between DR 23, which is an anionic diazo dye and is, therefore, negatively charged and the

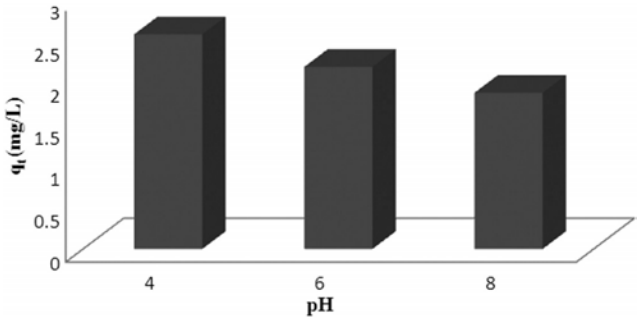

Fig 5 — Effect of solution *p*H on dye adsorption capacity ([DR 23] =20 mg/L, nZVI/MWCNT = 4 g/L, T=293 K).

partially negatively-charged nZVI/MWCNTs above pH_{zpc} (pH_{zpc} is the *p*H area in spaces where the catalyst surface charge is zero; 7.3). The increase in DR 23 dye adsorption when *p*H decreased is the result of protonation of the π electron-rich regions on the surface of the MWCNTs, which creates a positive surface charge. Under these conditions, the positively-charged surface sites on nZVI/MWCNTs favor the adsorption of DR 23 anions by electrostatic attraction[22]. However, hydroxide precipitation formed gradually when the solution *p*H was high; this blanketed the nZVI shell and decreased adsorption of DR 23[23].

Effect of temperature on DR 23 removal

The adsorption of DR 23 by nZVI/MWCNTs was conducted at an initial dye concentration of 20 mg/L at 20, 30 and 40°C. The effect of temperature on DR 23 dye adsorption capacity onto nZVI/MWCNTs was studied. It was observed that the adsorption of DR 23 increased by increasing the temperature from 20 to 40°C, confirming the endothermic nature of the adsorption reaction. This can be explained by the increased adsorptive interaction between the active sites of nZVI/MWCNTs and DR 23[24].

Equilibrium isotherm studies

To understand the nature of adsorption process, we have studied the equilibrium adsorption isotherms. When the amount of solute being adsorbed onto the adsorbent becomes equal to the amount being desorbed, the equilibrium concentration remains constant[25]. In this condition the distribution of solute between solution and adsorbent surface is expressed as a function of C_e and q_e at a fixed temperature called equilibrium adsorption isotherm. Several isotherm models have been used in this study. The isotherm parameters were evaluated using polymath 6.0 software and are shown in Table 1. To judge whether a model represents correctly the data, we

Table 1 — Isotherm constants for adsorption of DR 23 onto nZVI/MWCNTs (±95% confidence level)

Model	R^2	R^2_{adj}	S^2	Rmsd	Parameters	Parameter values
2-p Langmuir	0.9828762	0.9785953	0.0342718	0.0617088	q_m (mg/g)	3.721
					K_L (L/mg)	0.42068
2-p Freundlich	0.9361277	0.9201597	0.0019612	0.0147618	K_F (mg/g)	1.69
					n	4.125
2-p Temkin	0.9114126	0.8892658	0.0203825	0.0475891	RT/ΔQ	0.654
					K_T (L/mg)	9.351

have used correlation coefficient (R^2) and adjusted correlation coefficient (R^2_{adj}) parameters. If the correlation coefficient value was close to one and also close to (R^2_{adj}), it could be concluded that the regression model is correct. Average of observation ($\bar{y}$), R^2 and R^2_{adj} values were calculated by Eqs. (4)-(6), respectively:

$$\bar{y} = \frac{1}{n}(\sum_{i=1}^{n} y_{i_{obs}}) \quad \text{... (4)}$$

$$R^2 = 1 - \frac{\sum_{i=1}^{n}(y_{i_{obs}} - y_{i_{calc}})^2}{\sum_{i=1}^{n}(y_{i_{obs}} - \bar{y})^2} \quad \text{... (5)}$$

$$R^2_{adj} = 1 - \frac{(1-R^2)(n-1)}{n-p} \quad \text{... (6)}$$

where n is the number of observations, y_i is a specific observation, the notation "obs." relates to the observed data and notation "calc." relates to the calculated data. For comparing the various isotherm models in adsorption of DR 23 dye using nZVI /MWCNTs, we have also used variance (S^2) and Root mean square error (Rmsd) parameters. A model with smaller variance and Rmsd shows the data accurately. To calculate the values of Rmsd and S^2, Eqs. (7) and (8) have been used, respectively.

$$Rmsd = \frac{1}{n}\left(\sum_{i=1}^{n}(y_{i_{obs}} - y_{i_{calc}})^2\right)^{1/2} \quad \text{... (7)}$$

$$S^2 = \frac{\sum_{i=1}^{n}(y_i - y)^2}{n-1} \quad \text{... (8)}$$

The parameters of each model, R^2, R^2_{adj}, S^2 and Rmsd were calculated at 95% confidence interval for DR 23 dye adsorption onto the nZVI /MWCNTs nanoparticles and they are given in Table 1.

Langmuir isotherm

Langmuir isotherm[26] theory is based on the assumption that adsorption on the homogeneous surface, i. e. the surface consists of the identical sites, equally available for adsorption and with equal energies of adsorption and that the adsorbent is saturated after one layer of adsorbate molecules forms onto the surface[27]. The linearized form of the Langmuir adsorption isotherm equation is:

$$\frac{C_e}{q_e} = \frac{1}{K_L q_m} + \frac{C_e}{q_m} \quad \text{... (9)}$$

Figure 6(a) shows the Langmuir adsorption isotherm of the DR 23 onto nZVI /MWCNTs. As seen in Fig. 6(a) and Table 1 the Langmuir isotherm fits quite well with the experimental data (R^2= 0.9828). The maximum adsorption capacity (q_m), according to this model was 3.721 mg/g at 293 K. The fact that the Langmuir isotherm fits the experimental data very well may be due to homogeneous distribution of active sites onto nZVI /MWCNTs surface, since the Langmuir equation assumes that the surface is homogenous.

The essential characteristics of the Langmuir isotherm can be expressed in terms of a dimensionless constant separation factor or equilibrium parameter R_L, which is defined by the following equation[28]:

$$R_L = \frac{1}{1+K_L C_0} \quad \text{... (10)}$$

The R_L value indicates the type of the isotherm to be either irreversible (R_L=0), favorable (0<R_L<1), linear (R_L=1) or unfavorable (R_L>1). The plot of separation factor for different concentration (Fig. 6(b)) is indicative of the fact that in all equilibrium concentrations the adsorption of DR 23 dye is favorable.

Freundlich isotherm

Freundlich isotherm is an empirical equation that corresponds to the adsorption on the heterogeneous surfaces. It assumes that by increases in adsorbate concentration, the concentration of adsorbate on the adsorbent surface increases too. This isotherm model is applicable in both multi-layer (physisorption) and mono-layer (chemisorptions) adsorptions[29]. The linearized Feeundlich isotherm equationis given as:

$$lnq_e = ln\ _f + \frac{1}{n} lnC_e \quad \text{... (11)}$$

where C_e is the equilibrium concentration of solute (mg/L); and q_e, the equilibrium adsorption capacity

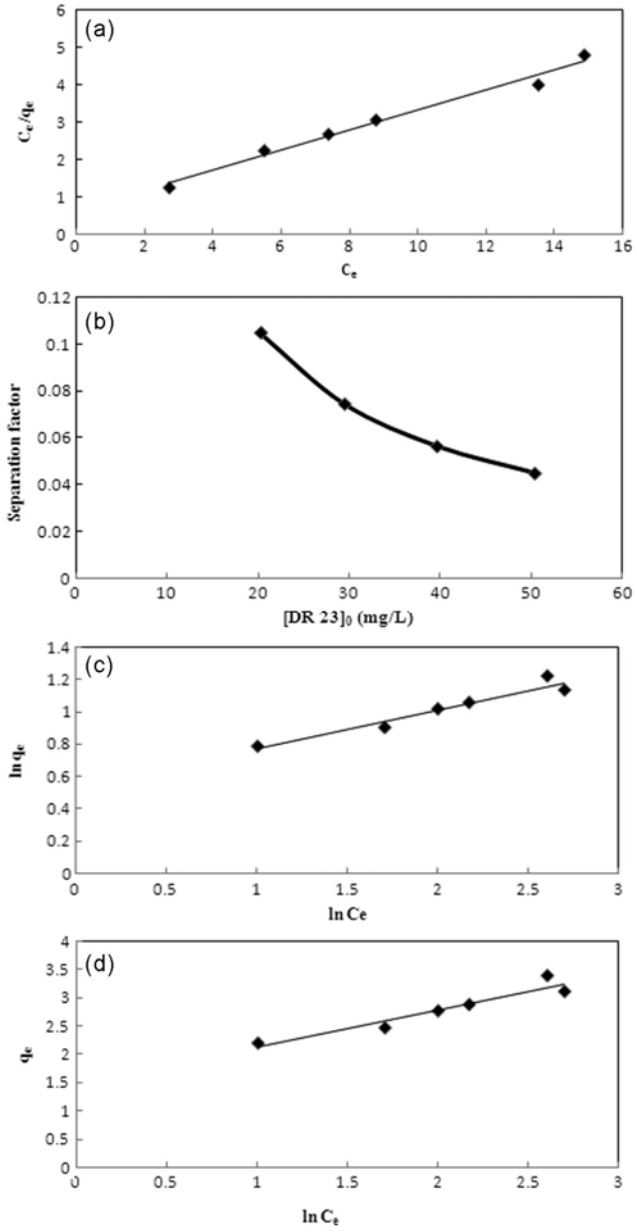

Fig. 6 — Plots of (a) Langmuir isotherm (b) Separation factor for different initial DR 23 concentration (c) Freundlich isotherm and (d) Temkin isotherm for DR 23 adsorption on nZVI/MWCNTs.

(mg/g), The Freundlich isotherm constants K_f shows the quantity of adsorbate adsorbed on to the adsorbent for a unit equilibrium concentration and the value of $(\frac{1}{n})$ indicates the heterogeneity of the system. In general, values n in the range of 1-10 illustrated that adsorbate was favourably adsorbed onto adsorbent; while n<1 indicated that adsorbate was unfavorably adsorbed onto adsorbent[30]. Results from Freundlich analysis shown in Table 2 indicating that DR 23 dye is favorably adsorbed onto nZVI /MWCNTs

Figure 6(c) shows the Freundlich isotherm of the DR 23 onto nZVI /MWCNTs. The R^2 value for this isotherm (R^2=0.9361) is not close enough to 1 and shows that Freundlich isotherm is not able to predict the experimental data in this work.

Temkin isotherm

The Temkin isotherm equation assumes that the heat of adsorption of all the molecules in the layer decreases linearly with coverage due to adsorbent-adsorbate interactions, and that the adsorption is characterized by a uniform distribution of the binding energies, up to some maximum binding energy. The linearized equation is[31]:

$$q_e = BlnK_T + BlnC_e \quad \ldots (12)$$

where $B = \frac{RT}{\Delta Q}$ is related to the heat of adsorption, T is the absolute temperature (K), R is universal gas constant (g/g mol K), ΔQ is the heat of adsorption (J) and K_T is the equilibrium binding constant (L/mg). Figure 6(d) shows the Temkin isotherm of the DR 23 adsorption onto nZVI /MWCNTs.

However R^2= 0.9114 in Table 1 indicate that Temkin model is not able to fit correctly the experimental data in adsorption of DR 23.

Adsorption kinetic studies

Adsorption kinetics can be useful in investigating the mechanism of adsorption and prediction of steps that control the rate of adsorption. Moreover, the obtained information from kinetic studies is used to select the best condition for dye removal process[32]. In fact the kinetic parameters are useful for designing and modeling the processes[33]. In this study, two kinetic models have been exploited to test the experimental data in adsorption of DR 23 dye. All the parameters of pseudo-first and pseudo-second order adsorption kinetic models and the intraparticle diffusion model were determined using polymath 6.0 software and are listed in Table 2. Similar to isotherm studies, for judging the goodness of fit, R^2, R^2_{adj}, S^2 and Rmsd values are calculated and given in Table 2. All parameters have been calculated at 95% confidence interval. The plots of experimental data and results obtained from two kinetic models and intra-particle diffusion model are shown in Fig 7(a), (b) and (c).

Lagergren's pseudo-first order kinetic model

The pseudo-first order or Lagergren first-order rate equation is based on the adsorption capacity[34] and is expressed by the following equation:

Table 2 — Kinetics model parameters value (±95% confidence level)

		Initial concentration (mg/L)			
		20	30	40	50
Pseudo-first-order kinetic model	k_1 (1/min)	0.5927119	0.5842217	0.5009979	0.4533337
	$q_{e,cal}$ (mg/g)	1.787691	2.350556	3.055496	3.070225
	R^2	0.9693484	0.9661884	0.9612914	0.9562696
	$\mathbf{R^2_{adj}}$	0.9616855	0.9577354	0.9516143	0.945337
	S^2	0.0486003	0.0522562	0.0442183	0.0675908
	Rmsd	0.0734849	0.0761987	0.0700938	0.0411166
Pseudo-second-order kinetic model	k_2(g/mg min)	0.300134	0.198862	0.201702	0.127139
	$q_{e,cal}$ (mg/g)	2.824061	3.672469	0.346469	3.789113
	R^2	0.9985332	0.9943554	0.9786983	0.9506062
	$\mathbf{R^2_{adj}}$	0.9980443	0.9924739	0.9715977	0.9341416
	S^2	0.0007772	0.0019299	0.0050701	0.0380477
	Rmsd	0.0096575	0.0152182	0.0246661	0.0120636
Intraparticle diffusion model	K_i	0.5453519	0.685164	1.034752	0.0970828
	C (mg/g)	0.9907803	1.23197	0.7567542	1.206285
	R^2	0.9420351	0.9978023	0.9943746	0.9869377
	$\mathbf{R^2_{adj}}$	0.9304421	0.9973627	0.9932495	0.9843253
	S^2	0.027646	0.0004241	0.0024843	0.0078989
	Rmsd	0.0075056	0.0065783	0.0159218	0.0283903

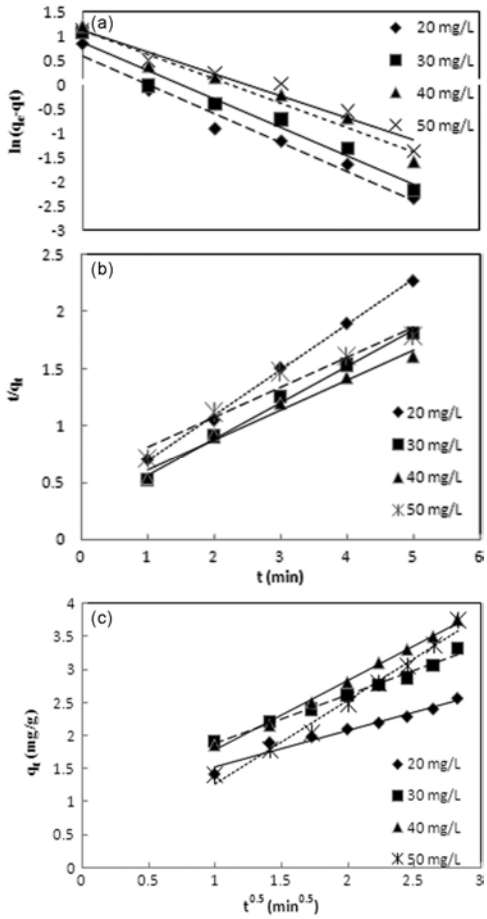

Fig 7 — (a) Pseudo-first-order kinetics model (b) Pseudo-second-order kinetics model (c) Intraparticle diffusion model of DR 23 onto nZVI/MWCNTs at 293 K.

$$\ln(q_e-q_t)=\ln(q_e)-k_1t \quad \text{... (13)}$$

where q_e and q_t are the amount of adsorbate adsorbed at equilibrium and at any time (mg/g), respectively, and k_1 is first order Lagergren model rate constant (1/min).

Pseudo-second order kinetic model

The pseudo-second order kinetic model assumes that the reaction rate is fast at first and became slower after reaching the equilibrium point and the reaction can continue for long time at this speed. This model is useful for explaining both of non-chemical and non-physical equilibriums and is based on the adsorption capacity of adsorbent[32]. Pseudo-second order kinetic model can be expressed by the following equation:

$$\frac{t}{q_t}=\frac{1}{k_2q_e^2}+\frac{t}{q_e} \quad \text{... (14)}$$

where q_e and q_t are defined as in the pseudo first-order model; and k_2, the rate constant of the pseudo second-order model for adsorption (g/mg min)[35]. According to the results in Table 2 it was concluded that the pseudo-second order kinetic model by greater correlation coefficients (R^2) and very small values of Rmsd and S^2 are in good agreement with experimental data in comparison with pseudo-first order kinetic model. A better fit to the pseudo-second order model suggests that the adsorption rate is dependent more on the availability of adsorption sites than the concentration of the DR 23 dye in solution[36]. The

kinetic models including pseudo-first-order and pseudo-second-order kinetic model for the adsorption of DR 23 dye on different adsorbents such as MWCNTS-Fe_3C[37], powdered TiO_2[38], mangrove bark[39] or U. Gambir green adsorbent[40] were examined. They found that experimental data better fits to pseudo-second order kinetic model compared to the pseudo-first order.

Mechanism of adsorption

The intra-particle diffusion model assumes the possibility of adsorbate transport into pores of adsorbent in batch mode adsorption[41]. Intra-particle diffusion model is expressed as[42]:

$$q = k_i t^{\frac{1}{2}} + C_i \quad \text{... (15)}$$

where C_i is the intercept which gives an idea about the boundary layer thickness. The large intercept value indicates the greater boundary layer effect; and k_i, the intra-particle diffusion rate constant (mg/g $min^{0.5}$), which can be evaluated from the slop of the linear plot of q versus $t^{\frac{1}{2}}$ [43]. According to this model, the plot of uptake should be linear if intra particle diffusion is involved in the adsorption process and if these lines pass through the origin then intraparticle diffusion is the rate controlling step. When the plots do not pass through the origin, this is indicative of some degree of boundary layer control and this further show that the intraparticle diffusion is not the only rate limiting step, but also other kinetic models may control the rate of adsorption, all of which may be operating simultaneously[44]. However, the linear plots (Fig. 7(c), Table 2) at each concentration did not pass through the origin. This indicates that the intraparticle diffusion was not only rate controlling step.

Thermodynamic studies

The spontaneity of a process can be determined by thermodynamic parameters such as enthalpy change (ΔH^o), free energy change (ΔG^o) and entropy change (ΔS^o). A spontaneous process will show a decrease in ΔG value with increasing temperature[45]. The thermodynamic parameters such as change in free energy (ΔG^o; J/mol), enthalpy change (ΔH^o; J/mol) and entropy change (ΔS^o; J/ mol K) are determined using the following relationships:

$$\Delta G° = T\Delta S° - \Delta H° \quad \text{... (16)}$$

$$\Delta G° = -RTlnK° \quad \text{... (17)}$$

$$K° = \frac{q_e}{C_e} \quad \text{... (18)}$$

$$lnK° = \frac{-\Delta H°}{RT} + \frac{\Delta S°}{R} \quad \text{... (19)}$$

where K^o is the equilibrium constant; T, absolute temperature (K); and R, gas constant. ΔH^o and ΔS^o values are obtained from the slope and intercept of plot $lnK°$ against 1/T. Figure 8 shows the effect of temperature on adsorption of DR 23 dye onto nZVI /MWCNTs nanocomposite (Van't Hoff plot). The observed thermodynamic values are listed in Table 3. The negative value of $\Delta G°$ at all temperatures indicate the spontaneous nature of the adsorption of DR 23 dye onto nZVI/MWCNTs. The negative values of Gibbs free energy change indicate that all the solutes are favored to stay in the stationary phase rather than in the mobile phase. The solute transfer from the mobile to stationary phase is enthalpically favorable. The positive value of ΔS showed the increased randomness at the solid-solution interfaces during the adsorption process and confirmed high preference of DR 23 adsorption onto nZVI /MWCNTs. However, the positive value of the change in enthalpy indicates that endothermic nature of adsorption. The pseudo-second order model is identified as the best kinetic model for the adsorption of DR 23 onto nZVI /MWCNTs nano particle surface. Accordingly, the rate constants (k_2) of the pseudo-second order model is adopted to calculate the activation energy of adsorption process using the following Arrhenius equation[24]:

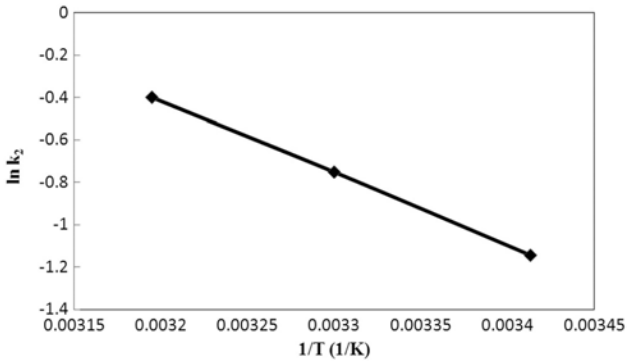

Fig. 8— Arrhenius plot for the adsorption of DR 23 onto nZVI/MWCNTs.

Table 3 — Thermodynamic parameters for the adsorption of DR 23 dye onto nZVI /MWCNTs nanoparticles

T	ΔG^o	ΔH	ΔS	R^2
K	kJ/ mol	kJ/ mol	J / mol K	
298	-0.37906	40.68182	140.2652	0.99746
308	-1.90085	-	-	-
318	-3.17785	-	-	-

Table 4 — Activation energy for the adsorption of some dyes from aqueous solution

Adsorbent	Dye	E_a (kJ/mol)	Reference
MWCNTs-Fe_3C	DR 23	15	[37]
CNTs	Procion Red MX-5B	33.35	[47]
CNTs	Direct Red 224	12.13	[48]
CNTs	Direct yellow 86	9.62	[48]
CNTs	Methylen blue	18.54	[49]

$$lnk_2 = lnA - \frac{E_a}{RT} \quad \ldots (20)$$

where k_2 (g /mg min) is the rate constants for the pseudo-second order adsorption kinetics, A (g/mg min) is the temperature-independent Arrhenius factor, E_a (kJ/mol) the activation energy, R (8.314 J/mol K) is the gas constant and the T (K) is the temperature. The activation energy could be determined from the slope of the plot of lnk_2 versus 1/T. The activation energy is found to be 28.3765 kJ/mol (R^2 =0.9998) at 293 K for DR 23 adsorption onto nZVI /MWCNTs nanoparticles surface. The magnitude of the activation energy yields information on whether the adsorption is mainly physical or chemical. The physisorption process usually has energies in the range 5-40 kJ/mol, while higher activation energies (40-800 kJ/mol) suggest chemisorptions[46]. The value of activation energy given confirms the nature of the physisorption process of DR 23 onto nZVI /MWCNTs adsorbent. Table 4 shows the activation energy for the adsorption of some dyes from aqueous solutions that have been reported in several articles.

Furthermore, ΔG^o for physisorption is less than that for chemisorptions. The change in free energy for physisorption is between -20 and 0 kJ/mol, the physisorption together with chemisorptions is at the range of -20 to -80 kJ/mol and chemisorption is at the range of -80 to -400 kJ/mol[50]. The values of ΔG^o (-0.37 to -3.17 kJ/mol) for the adsorption of DR 23 onto nZVI /MWCNTs were in the range of physisorption.

Conclusion

The results of the present study show that nZVI/MWCNTS nanoparticles can be successfully used as an adsorbent for quantitative removal of DR 23 from aqueous solutions. Equilibrium data are fitted well in the Langmuir model of adsorption, showing monolayer coverage of DR 23 molecules at the outer surface of nZVI/MWCNTS nanoparticles. The value of R_L is found between 0 and 1, which confirms that the nZVI/MWCNTS nanoparticles are favorable for adsorption of DR 23 dye. Furthermore, according to the results obtained from the comparsion of kinetic models, the pseudo-second-order kinetic model had the closest agreement with the experimental data which suggests that the adsorption rate is dependent more on the availability of the adsorption sites than the concentration of the DR 23 in the solution. Thermodynamic parameters indicate spontaneous and endothermic process.

References

1 Crini G, *Bioresource Technol*, 97 (2006) 1061.
2 Zollinger H, *Color chemistry: Synthesis, Properties and application of organic dyes and pigments*, (Chemistry VCH, Weinheim), 1991, 92.
3 Bauer C, Jacques P & Kalt A, *Chem Phys Lett,* 307 (1999) 397.
4 Arslan I, Balcioglu I A & Bahnemann D W, *Dyes Pigm*, 47 (2000) 207.
5 Gillham R W & O Hannesin S F, *Ground water*, 32 (1994) 958.
6 Theron J, Walker J A & Cloete T E, *Crit Rev Microbial*, 34 (2008) 43.
7 Ramakrishna K R & Viraraghvan T, *Water Sci Technol*, 36 (1997) 189.
8 Zhang Y, Jing Y, Quan X, Liu Y & Onu P, *Water Sci Technol*, 63:4 (2011) 741.
9 Saxe J P, Lubenow B L, Chiu P C, Huang C P & Cha D K, *Water Environ Res*, 78 (2006) 19.
10 Liu T, Wang Z L, Zhao L & Yang X, *Chem Eng J*, 189 (2012) 196.
11 Sakulchaicharoen N, Carroll D M O, Herrera J E, *J Contam Hydrol*, 118 (2010) 117.
12 Greenlee L F & Hooker S A, *Desalin Wat Treat*, 37 (2012) 114.
13 Rahbari M & Goharrizi A S, *Water Environ Res*, 81 (2009) 598.
14 Zhang S, Wang D, Zhou L, Zhang X, Fan P & Quan X, *Chem Eng J*, 217 (2013) 99.
15 Liu X, Wang M, Zhang S & Pan B, *J Environ Sci*, 25 (7) (2013) 1263.
16 Wang W, Zhou M H, Mao Q, Yue J J & Wang X, *Catal Commun*, 11(2010) 937.
17 Sohrabi M R, Mansouriieh N, Khosravi M & Zolghadr M, *Water Sci Technol*, 71 (9) (2015) 1367.
18 Mansouriieh N, Sohrabi M R & Khosravi M, *Arabian J Chem*, (2015), DOI: 10.1016/j.arabjc.2015.04.009.
19 Mourabet M, Rhilassi A E, Boujaady H E, Bennani-Ziatni M & Taitai A, *Arabian J Chem*, 2014 Doi. 10.1016.
20 Fan J, Zhang J, Zhang C, Ren L & Shi Q, *Desalination*, 267 (2011) 139.
21 Gonen F & Serin S, *Afr J Biotechnol*, 11 (2012) 1250.
22 Lin K S, Chang N B & Chuang T D, *Sci Tech Adv Mater*, 9 (2008) 1.
23 Venkatapathy R, Bessingpas D G, Canonicia S & Perlinger J A, *Appl Catal B*, 37 (2002) 139.
24 Dogan M & Alkan M, *Chemosphere*, 50 (2003) 517.
25 Kundu S & Gupta A K, *Chem Eng J*, 122 (2006) 93.
26 Hameed B H, *J Hazard Mater*, 162 (2009) 344.

27 Walker G M & Weatherley L R, *Chem Eng J*, 83 (2001) 201.
28 Malkoc E & Nuhoglu Y, *Chem Eng Process*, 46 (2007) 1020.
29 Boparai H K, Joseph M & O Carrol D M, *J Hazard Mater*, 186 (2011) 458.
30 Gupta V K, Ali I & Saini V K, *J Colloid Interf Sci*, 315 (2007) 87.
31 Temkin M J, Pyzhev V, *Acta Physiochim*, URSS. 12 (1940) 217.
32 Febrianto J, Kosasih A N, Sunarso J, Ju Y H, Indraswati N & Ismadji S, *J Hazard Mater*, 162 (2009) 616.
33 Hameed B H, Tan I A W & Ahmad A L, *Chem Eng J*, 144 (2008) 235.
34 Oubagaranadin J U K & Murthy Z, *Chem Prod Process Model*, 4 (2009) 32.
35 Wang S & Zhu Z H, *Dyes Pigm*, 75 (2007) 306.
36 Liu Y, *Colloids Surf A*, 320 (2002) 75.
37 Konicki W, Pelech I, Mijowska E & Jasinska I, *Chem Eng J*, 210 (2012) 87.
38 Holliman P J, Velasco B V, Butler I, Wijdekop M & Worsley D A, *Int J Photoenergy*, (2008) 1.
39 Tan L S, Jain K & Rozaini C A, *J App Sci Environ Sanit Sby*, 5 (3) (2010) 283.
40 Achmad A, Kassim J, Suan T K, Amat R C & Seey T L, *J Phys Sci*, 23 (1) (2012) 1.
41 Sheel T & Arthoba Nayaka Y, *Chem Eng J*, 191 (2012) 123.
42 Demirbas E, Kobya M, Oncel M S & Sencan S, *Bioresour Technol*, 84 (2002) 291.
43 Ozcan A, Oncu E M & Ozcan A S, *Colloid Surf A*, 277 (2006) 90.
44 Hameed B H & Daud F B M, *Chem Eng J*, 139 (2008) 48.
45 Ngah W W & Hanafiah M, *J Biochem Eng*, 39 (2008) 521.
46 Nollet H, Roels M, Lutgen P, Meeren P V D & Verstraete W, *Chemosphere*, 53 (2003) 655.
47 Wu C-H, *J Hazard Mater*, 144 (2007) 93.
48 Kuo C Y, Wu C H & Wu J Y, *J Colloid Interf Sci*, 327 (2008) 308.
49 Yao Y, Xu F, Chen M, Xu Z & Zhu Z, *Bioresour Technol*, 101 (2010) 3040.
50 Jaycock M J & Parfitt G D, Chemistry of Interfaces (Ellis Horwood Ltd., Onichester) 1981.